Int. J. Solids Structures Vol. 19, No. 4, pp. 357–373, 1983
Printed in Great Britain.

0020-7683/83/040357-17$03.00/0
Pergamon Press Ltd.

NON-HERTZIAN CONTACT STRESS ANALYSIS FOR AN ELASTIC HALF SPACE—NORMAL AND SLIDING CONTACT

N. AHMADI, L. M. KEER and T. MURA
Department of Civil Engineering, Northwestern University, Evanston, IL 60201, U.S.A.

(*Received* 6 *November* 1981; *in revised form* 16 *June* 1982)

Abstract—A general method of numerical solution in the non-Hertzian elastic contact problem is developed using rectangular subdivisions. The major application of the method given is in the sliding contact of a short rough cylinder with an elastic half space; the contact region is the side of the cylinder, whose axis may not be exactly aligned to the surface of the half space. The stress singularity at the ends of the cylinder is taken as either square root (to determine stress intensification factor) or is approximated by compact elements to reduce computing time. An iterative scheme is used and the convergence to the unknown shape of the contact region is rapid.

INTRODUCTION

The problem of the contact of smooth elastic bodies under normal loading was first investigated by H. Hertz[3] in 1881. He computed and verified by experiment the load distributions over the contact area and solved for the stresses in the body through use of the Newtonian potential function. Tomas and Hoersch[15] transformed the Hertzian solution for the stresses on the axis of symmetry into elliptic integrals and found that shearing stresses on the axis of symmetry are maximum at some distance under the center of the contact area. Mindlin[10] investigated the distribution of tangential load across the area of contact, when one elastic body slides over another identical elastic body. He found that the stress on the boundary of the contact area due to tangential load is infinite if there is no slip; hence, the maximum value that the stress can have is limited by the Amontons–Coulomb law.

Kalker[5], through the use of asymptotic expansions for certain surface displacement integrals, solved the non-Hertzian contact problem for the case where the contact area was long in the y-direction and narrow in the x-direction, where x, y, z is a rectangular coordinate system with the z-axis perpendicular to the surface. Kalker found the shape of the contact area if a finite cylinder whose axis is parallel to the half space is pressed into the half space, except for the region near the tips.

Recently, the emphasis has been to employ numerical techniques to solve a large variety of contacting body shapes that represent practical situations. Conry and Seireg[1] were among the first to solve the contact problems by using a mathematical programming scheme to minimize the potential energy of contact. Later, Singh and Paul[4] employed the flexibility method of analysis to derive a system of linear equations in terms of unknown contact pressures. The system proved to be an ill-conditioned system of linear equations. Most recently, Oh and Trachman[11] extended Conry's method to the contact of cylinders which were partially crowned at the ends and determined the pressure distribution between them for certain cases of symmetry. Hartnett[2] employed a new technique of numerical solutions for counter-formal elastic bodies in contact problems. He used the flexibility method of analysis with the Boussinesq half space force-displacement relations. Recent work by Kalker[6] has successfully applied variational principles to the problems of rolling contact.

In the present method an iterative approach is developed that extends the scheme of Hartnett. The parameters, which should be checked after each iteration, have been reduced to one. In addition, the shear force has been included into this numerical approach, and reasonable results have been obtained for several contact shapes; particular emphasis in this study has been devoted to the indentation of a finite circular cylinder, whose axis is parallel to the half space and whose side makes the contact. If the cylinder has a sharp edge (90°), then there will be singular behavior in the vicinity of the edge.

The present approach converges to approximate the true solution after about four to five

iterations. This convergence exists for an initial guess whose area is larger than the true contact area Ω.

The new method is roughly equally accurate as the relatively slow numerical method of Paul and Hashemi[12], and the fast Reusner type methods[13, 8].

METHOD OF SOLUTION

We will consider the case of contact in which two bodies are first pressed normally against each other and then are made to slide tangentially. The tangential motion is assumed to be sufficiently great that the tangential stresses will be in the direction of the motion irrespective of the initial surface displacements caused by slip. The tangential stresses will be related to the normal stresses by means of the Amontons–Coulomb friction law. It is recognized that the normal displacements caused by the tangential stresses will cause a change in the contact region in addition to that caused by the normal load and the geometry of the bodies.

In the solution of the general problem we will make use first of the solutions by Boussinesq and by Cerruti (see[9]).

Formulation of smooth contact problem

The contact problem may be formulated by the following considerations. Let two bodies, 1 and 2, be initially in contact at point 0, which is considered as the origin of $x0y$ coordinates in the common tangent plane between two bodies. We first assume that there is only a normal load over the contact area Ω. In Fig. 1(a) the separation function between the two bodies before contact and in Fig. 1(b) after contact are, respectively, $f(x, y)$ and $e(x, y)$. The following conditions must be satisfied:

$$p(x, y) \geq 0 \quad (x, y) \in \Omega \tag{1}$$

$$p(x, y) = 0 \quad (x, y) \notin \Omega \tag{2}$$

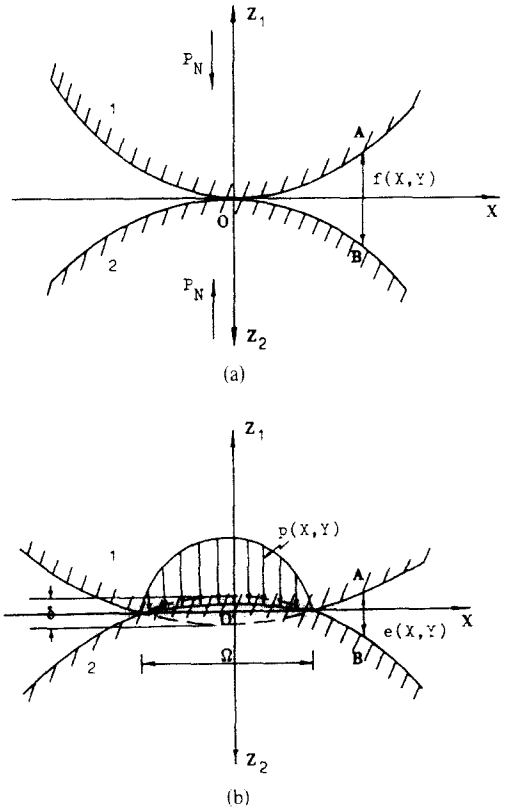

Fig. 1. Contact of two elastic bodies before and after the application of load.

$$e(x, y) = 0 \quad (x, y) \in \Omega \tag{3}$$

$$e(x, y) \geq 0 \quad (x, y) \notin \Omega. \tag{4}$$

If two points on the z_1 and z_2 axes in the two bodies far from the contact region are brought together by a distance δ, which is the relative approach, then the distance of two points A,B(AB is parallel to the z-axis, the common normal of the two bodies at point 0) on the surface of the two bodies will change from $f(x, y)$ to $e(x, y)$ through the relation:

$$e(x, y) = f(x, y) + u_{1z}^N + u_{2z}^N - \delta \tag{5}$$

where u_{1z}^N and u_{2z}^N are normal displacements of the two bodies at points A,B due to force P_N. Since the load-displacement relation on the surface can be taken from Love[9], we note here that

$$u_{z|z=0}^N = \frac{P_N(1-\nu)}{2\pi G} \cdot \frac{1}{R} \tag{6}$$

$$u_{z|z=0}^S = \frac{P_s(1-2\nu)}{4\pi G} \cdot \frac{x}{R^2}. \tag{7}$$

In the simpler case that there is no shear, then our main interest will be eqn (6), from which the contact problem can be obviously formulated as

$$e(x, y) = f(x, y) + K_1 \int\int_\Omega \frac{p(x', y')\,dx'\,dy'}{\sqrt{(x-x')^2 + (y-y')^2}} - \delta \tag{8}$$

where K_1 is an elastic parameter, defined as

$$K_1 = \frac{1-\nu_1}{2\pi G_1} + \frac{1-\nu_2}{2\pi G_2} \tag{9}$$

where ν_1, ν_2, G_1, G_2 are Poisson's ratios and moduli of rigidity for the two bodies, respectively.

By definition of eqns (1)–(4), for $x, y \in \Omega$, $e(x, y) = 0$, and eqn (8) becomes an integral equation with unknowns $p(x, y)$, δ, Ω where by the use of the equilibrium condition

$$\int\int_\Omega p(x', y')\,dx'\,dy' = P_N \tag{10}$$

and the condition that $p(x, y) \geq 0$ in Ω an analytical solution can be obtained for the elliptic case and numerical methods can be used for more complicated contacting objects.

Numerical solution

The method of numerical solution is the following for the problem of frictionless contact. Consider an initial covering of the contact area to be a rectangle of size $2NA \times 2NB$, which is divided into $N \times L$ small rectangular patches with area $2A \times 2B$. This covering is chosen such that the contact region Ω is overestimated. The covering and Ω are shown in Fig. 2(a). In order to solve the integral equation (8) with $e(x, y) = 0$

$$K_1 \int\int_\Omega \frac{p(x', y')\,dx'\,dy'}{\sqrt{(x-x')^2 + (y-y')^2}} = \delta - f(x, y) \tag{11}$$

we assume that the pressure at each path j is of constant value P_j. Then, eqn (11) will be given in the form

$$K_1 \sum_{j=1}^{k'} F_{ij} P_j = \delta - f_i, \quad i = 1, \ldots, k' \tag{12}$$

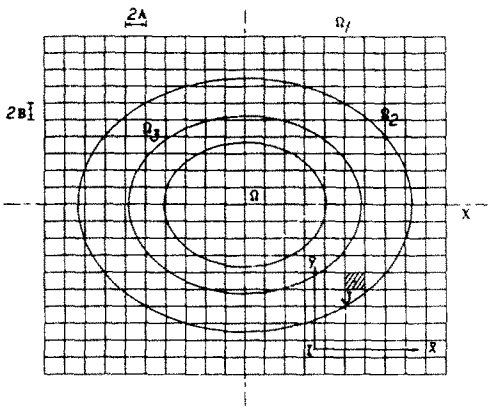

2(a)

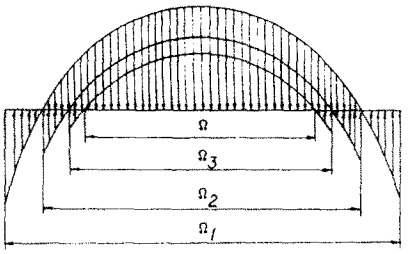

2(b)

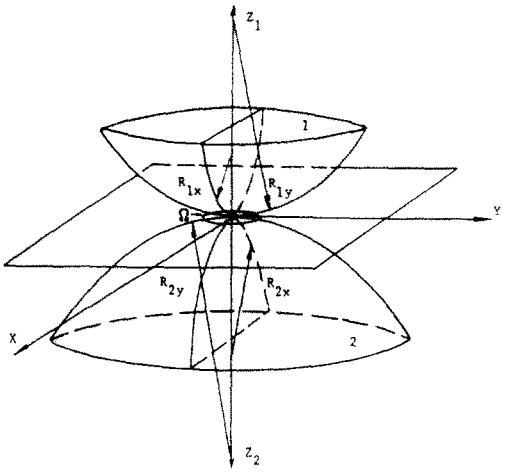

2(c)

Fig. 2. Method of discretization of the contact area.

where k' is the number of patches in Ω, F_{ij} is an influence function, and f_i is $f(x_i, y_i)$. The influence function F_{ij} is the displacement K_1 at point i due to the distribution of unit normal load on element j and can be calculated as

$$F_{ij} = \int_{\bar{x}-A}^{\bar{x}+A} \int_{\bar{y}-B}^{\bar{y}+B} \frac{dx\,dy}{R} \tag{13}$$

$$= [f_1(\bar{x}+A, \bar{y}+B) + f_1(\bar{x}-A, \bar{y}-B) - f_1(\bar{x}-A, \bar{y}+B) - f_1(\bar{x}+A, \bar{y}-B)],$$

where

$$f_1(x, y) = x \log(R+y) + y \log(R+x), \quad R = \sqrt{x^2+y^2}, \tag{14}$$

$2A \times 2B = S$ is the area of patch j, and $\bar{x}$, $\bar{y}$ are coordinates of the center of patch j with respect to the center of patch i. We also note that the assumption is made that the displacement at the center of the patch represents the actual displacement, which becomes more accurate as the subdivisions are made smaller. Furthermore, the condition of global equilibrium is

$$\sum_{j=1}^{k'} P_j = P_N/S. \tag{15}$$

Thus, we have k' linear equations generated by eqns (12), (13), and conditions (1)–(4) (equivalent to $p(x, y) \geq 0$) in Ω. The unknowns are the following: pressures P_j, δ, and k'. In the first iteration we assume that $k' = k_1 = N \times L$ and Ω_1 to be a covering of size 2NA by 2LB. Since the contact area is larger than the actual one, some of the pressures P_j near the boundary of Ω_1 will be negative (Fig. 2b).† The following set of $k_1 + 1$ equations can be solved for the unknowns $P_j (j = 1, \ldots, k_1)$ and δ:

$$K_1 \sum_{j=1}^{k'} F_{ij} P_j - \delta = -f_i \tag{16}$$

$$\sum_{j=1}^{k'} P_j = P_N/S. \tag{15}$$

Here, we assume that P_N is known. Since a portion of the P_j's will be negative, then the actual maximum stress will be overestimated. Furthermore, we have for the sum of the positive loads, $\Sigma_{j=1}^{k'} P_j > P_N/S$ $(P_j > 0)$. Thus, the area over which the positive P_j's act also overestimates the actual Ω.

For the next iteration we set those P_j's which are negative equal to zero and consider the number of P_j's which are positive to be k_2 and Ω_2 to be the corresponding area. We now have $k_2 + 1$ equations for the corresponding $k_2 + 1$ unknowns. The procedure is continued until $k_{n+1} = k_n = k'$. We note that if the problem possesses symmetries that can be determined a priori, then the number of equations can be reduced (or the patches can be made smaller) thereby increasing the accuracy.

NUMERICAL SOLUTION INCLUDING FRICTION

For the case of friction we also have, in addition to the normal force P_j in each subdivision, a shear force μP_j, where μ is the coefficient of static friction. We assume that the direction of this force is the same as the direction of motion of the two bodies relative to each other. The effect on the normal displacements is to change eqn (5) to

$$e(x, y) = f(x, y) + u_{1z}^N + u_{2z}^N + u_{1z}^S + u_{2z}^S - \delta \tag{17}$$

where u_{1z}^S and u_{2z}^S are of the form given in relation to tangential load by eqn (7). From eqn (17) with $e(x, y) = 0$ the integral equation becomes

$$K_1 \int\int_\Omega \frac{p(x', y')\,dx'\,dy'}{\sqrt{(x-x')^2 + (y-y')^2}} + K_2 \int\int_\Omega \frac{(x-x')p(x', y')\,dx'\,dy'}{(x-x')^2 + (y-y')^2} = \delta - f(x, y), \; x, y \in \Omega \tag{18}$$

where Ω is the contact region and K_2 is defined as

$$K_2 = \frac{(1-2\nu_1)\mu}{4\pi G_1} - \frac{(1-2\nu_2)\mu}{4\pi G_2}. \tag{19}$$

Here, we note that the minus sign in eqn (19) is due to antisymmetrical nature of the Cerruti solution [9].

†The edge pressures are actually singular, but they are being approximated by the loads over finite patches.

Equation (18) leads to the following equation, similar to eqn (16) given earlier:

$$K_1 \sum_{j=1}^{k'} F_{ij}P_j + K_2 \sum_{j=1}^{k'} F'_{ij}P_j = \delta - f_i, \quad i = 1, \ldots, k', \tag{20}$$

where also eqn (15) must be used. The influence function F'_{ij} can be easily determined as

$$\begin{aligned} F'_{ij} &= \int\int_S \frac{x\,dx\,dy}{x^2+y^2} \\ &= f_2(\bar{x}+A, \bar{y}+B) + f_2(\bar{x}-A, \bar{y}-B) - f_2(\bar{x}-A, \bar{y}+B) - f_2(\bar{x}+A, \bar{y}-B) \end{aligned} \tag{21}$$

where

$$f_2(x, y) = y \log R + x \tan^{-1}\frac{y}{x}, \quad R = \sqrt{x^2+y^2}. \tag{22}$$

We can write the solution in the form

$$K_1 \sum_{j=1}^{k'} \bar{F}_{ij}P_j = \delta - f_i \tag{23}$$

where

$$\bar{F}_{ij} = F_{ij} + F'_{ij}K_2/K_1. \tag{24}$$

The method of solution is the same as with the frictionless problem. However, we note that in this case the pressure distribution over the contact area may be symmetric only with respect to the direction in which the shear is assumed to be applied. Therefore, we can reduce the size of the linear equations at most by half. The matrix $\bar{F}_{ij}$ is not symmetric, since although the influence function for the normal load is symmetric, the one for the shear load is antisymmetric.

Effect of sharp edge

If there are no sharp edges in the contact area, the values of P_j's are finite; however, for the case in which a sharp edge appears, as in the contact between a short rigid cylinder and an elastic half space, the values of the P_j's become infinite as a square root near this edge. We consider the pressure to vary with the distance of the point to the sharp edge as

$$P_j = \frac{P'_j l}{\sqrt{l^2 - y_1^2}} = \frac{P'_j l}{\sqrt{(2l-y)y}} \tag{25}$$

in which $2l$ is the length of the cylinder, and P'_j is assumed to be constant for element j, and y represents the distance between each point of element j and the sharp edge (Fig. 3a). For this case the stiffness matrix becomes

$$F''_{ij} = \sum_{\bar{y}-B}^{\bar{y}+B} \frac{\ln\left[\dfrac{\bar{x}+A+\sqrt{(\bar{x}+A)^2+\bar{y}_1^2}}{\bar{x}-A+\sqrt{(\bar{x}-A)^2+\bar{y}_1^2}}\right] l}{\sqrt{(2l-\bar{y}_1-y_i)(\bar{y}_1+y_i)}}\,d\bar{y}_1. \tag{26}$$

The one-dimensional integral above must be integrated numerically, and we use the Gauss–Legendre quadrature method with 16 weighting points. In eqn (26) $\bar{x}$, $\bar{y}$ are coordinates of the point j with respect to point I, $\bar{x} = x_j - x_i$, $\bar{y} = y_j - y_i$, A, B are the half size of element j. The equilibrium equation will also change to

$$P_N = \sum_{j=1}^{k'} 2AP'_j \sum_{\bar{y}-B}^{\bar{y}+B} \frac{d\bar{y}_1\, l}{\sqrt{(2l-\bar{y}_1-y_i)(\bar{y}_1+y_1)}} \tag{27}$$

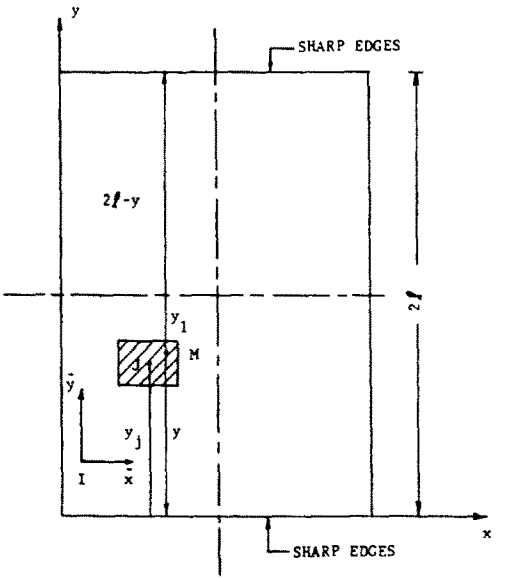

3(a)

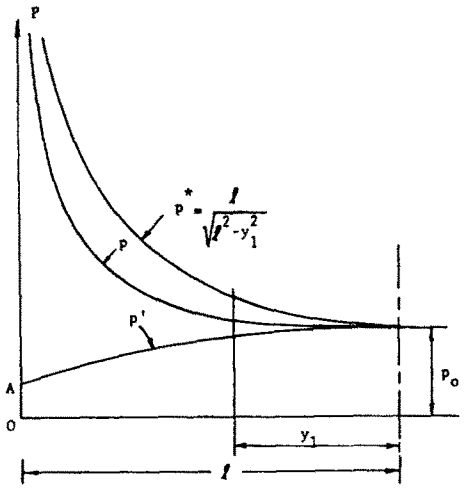

3(b)

Fig. 3. Method of discretization of the contact area with consideration of singular edge stresses.

or through the change of variable, $\cos u = 1 - (\bar{y}_i - y_j)/l$, (27) becomes

$$P_N = \sum_{j=1}^{k'} F''_{k+1,j} P'_j \tag{28}$$

where

$$F''_{k+1,j} = \left[\cos^{-1}\left(1 - \frac{y_j + B}{l}\right) - \cos^{-1}\left(1 - \frac{y_j - B}{l}\right)\right] 2Al. \tag{29}$$

After a number of iterations with the same approach use as before, we obtain a set of P_j's, where their value for edge elements is finite and smooth.

In Fig. 3(b) the centerline pressure distribution of the cylinder in contact, p, p', and the function $p^* = l/(l^2 - y_1^2)^{1/2}$ have been shown. These three plots are related by the equation

$$p = p'p^*. \tag{30}$$

Thus, by having been given p' and p^*, the curve for p can be obtained from eqn (30). Let the curvatures of the cylinder in two directions be RC_x, RC_y, where $RC_x = 1/R$ and $RC_y = 0$ for a straight cylinder. For this case the value of p' at the edges is OA; for $RC_y > 0$, point A will have a reduced value and may even become zero; for $RC_y < 0$, point A will have a higher value. The center line pressure distribution of the cylinder in contact, for different values of $RC_y > 0$ is shown in Fig. 6(c).

We note also that when an edge is in contact with a half space, such as for a finite cylinder, then the cylinder must be assumed to be *rigid*. This is because of the utilization made of the elasticity solutions for the deformation of a *half space*. If both the cylinder and half space were elastic, then a quarter space solution would be the appropriate one for describing the elastic response of the cylinder.

Shape of contact region

Each row or column of pressure distribution in the contact area can be covered by a special function which passes through them all and has in addition an infinite slope at the intersection with the contact plane. This function is in the form of

$$F_c(x) = \sqrt{\sum_{i=1}^{N} l_i(x) P_i^2} \tag{31}$$

where the weight function $l_i(x)$ is

$$l_i(x) = \prod_{\substack{j=1 \\ j \neq i}}^{N} \left(\frac{x^2 - x_j^2}{x_i^2 - x_j^2} \right). \tag{32}$$

The function $F_c(x)$ is symmetric with respect to the P-axis and the number of data points is $2N$. The data points are suitable for contact indenters having no sharp edges; i.e. if the axis of the cylinder is in the y-direction, the data points are smooth in the x-direction, and if it is crowned in the y-direction, then the function $F_c(x)$ can also be used in that direction.

For $N = 2$, $F_c(x)$ gives the equation of the ellipse exactly, as expected. The value of x_0, where $F_c(x_0) = 0$, can be determined for each row; finally, by having known values of (x_0, y_0), where y_0 is the coordinate of the same row, the contact area can be plotted.

RESULTS

The technique of numerical solution developed earlier in this work can be applied to a wide range of smooth and rough contact problems having different contact shapes. First, for verification of the present method, we apply the comparison case of the Hertz solution. The shapes of the two bodies in contact can be considered with good accuracy to be given by the quadratic form for the surfaces as

$$f(x, y) = \left(\frac{1}{2R_{1x}} + \frac{1}{2R_{2x}} \right) x^2 + \left(\frac{1}{2R_{1y}} + \frac{1}{2R_{2y}} \right) y^2$$

where R_{1x}, R_{2x}, R_{1y}, R_{2y} are the principal radii (min. and max.) of the two bodies, respectively. Furthermore, if we assume that $R_{2x} = R_{2y} = \infty$ and $R_{1x} = 50.8$ mm (2 in.), $R_{1y} = 101.6$ mm (4 in.), then, body 1 is an ellipsoid indenting body 2, which is a half-space. Body 1 can be regarded as a fully crowned cylinder with radius R_{1x} and crown radius R_{1y}. The bodies will be assumed to be made from steel with compliance

$$K_1 = \frac{1 - \nu_1}{2\pi G_1} + \frac{1 - \nu_2}{2\pi G_2} = 2.76 \times 10^{-6}/\text{MPa} = (1.9 \times 10^{-8}/\text{psi}).$$

The total load applied to compress the two bodies is $P = 88.96$ kN (20000 lb.). Using the results of the well-known solution for elliptic contact the first choice for a blanket is given as 10.16 mm by 10.16 mm (0.4 in. by 0.4 in.), which is divided into 20 by 20 patches having the size of

0.508 mm × 0.508 mm (0.02 in. by 0.02 in.). The results are given in the following Table:

Table.

	a = Semi Maj. Axis	b = Semi Min. Axis	P_0 = Max. Pressure	δ = Relative Approach
Hertz Solution	4.318 mm (0.170″)	2.743 mm (0.108″)	3592.3 MPa (52.10×10^4 psi)	0.166 mm (0.006522″)
Presented Num. Solution	4.369 mm (0.172″)	2.819 mm (0.111″)	3597.8 MPa (52.18×10^4 psi)	0.166 mm (0.006523″)

The numerical results are in very good agreement with the analytical Hertz solution and the maximum relative error for the size of the contact area is less than 3% and for pressure is less than 0.15%. We note that the results are given in terms of their physical quantities rather than dimensionless values. Future test cases will involve stress distributions and contact stress distributions that require numerical characterization since these quantities cannot be put into simple dimensionless forms. Figure 4(a) shows the pressure distribution between body 1 and the half space, body 2, where the shape of the contact areas is compared in Fig. 4(b). Figures 4(c, d) show the comparison of the pressure along the center line calculated by the present method as compared with the Hertz solution. In Fig. 4(e) a frictional shear stress is added† ($\mu = 0.5$) and the normal stress is seen to change only slightly along the centerline. The contact area (not shown) is similarly changed only slightly. The next examples are those in which the solution is not known.

Aligned cylinder (frictionless).

Here, body 1 is a short rigid cylinder with $R_x = 50.8$ mm (2.0 in.), $R_y = \infty$, and total length $l = 12.70$ mm (0.50 in.) which is equal to the length of a blanket with 10 by 20 divisions and a total load $P = 26.70$ kN (6000 lb.). Figures 5(a, b) show the pressure distribution and contact area for this case. The edge stresses are not taken as singular; instead, more compact patches are considered at the edges. Although the correct stress distribution is therefore only approximated, it appears that the overall accuracy (except in the determination of stress intensification factor) is not affected.

The singularity at the end of the cylinder can be considered as having the form $(l^2 - y^2)^{-1/2}$, where y is the distance from the middle of the cylinder. Then, by assuming constant $p'(x, y)$ instead of $p(x, y)$ in eqn (11) in each patch and solving eqn (12) for P'_j with P''_{ij}, which is described in eqn (26), the results of calculating the P' distribution over the contact area are numerically described as shown in Fig. 6(a, b). The cylinder in Fig. 6(a) has $R_x = 50.8$ mm (2.0 in.), $R_y = \infty$, $l = 12.70$ mm (0.5 in.), and a total load $P = 26.70$ kN (6000 lb.), and the cylinder in Fig. 6(b) has $R_x = 50.8$ mm and $R_y = -762$ mm (−30. in.) with a total load $P = 26.70$ kN. This case was also tested with more compact elements at the edges but no changes were observed, since the p' distribution has no singularities over the entire contact. For calculating the pressure distribution over the contact area, the following equation can then be used

$$p(x, y) = lp'(x, y)/(l^2 - y^2)^{1/2}.$$

Aligned cylinder (experiment)

In order to test the accuracy of the calculation for the determination of the contact region a modest experiment was performed. A thick sheet of polyurethene rubber was glued to a flat base ($E = 3.45$ MPa (500 psi), $\nu = 0.474$). The rubber was coated with pumice powder and then indented by aluminum cylinders $l = 12.7$ mm (0.5 in.), $R = 12.7$ mm (Fig. 7a) and $l = 139.7$ mm (5.5 in.), $R = 12.7$ mm (Fig. 7b). The pumice was cleanly removed by the contact of the cylinder and as has been seen by the two figures the agreement between theory and experiment is excellent. The contact is seen to slowly vary and achieves its greatest width near the sharp edges of the cylinder. Figure 7(c) shows the pressure distribution for the cylinder of Fig. 7(a), uncorrected for singularity behavior at the edge.

†Here we assume one of the bodies (body 2) to be a rigid half space to calculate the effect of the shear.

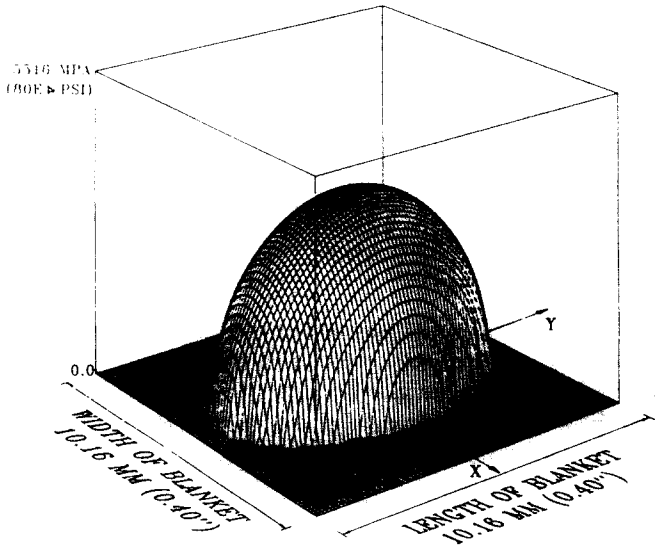
0.0
Y
X
WIDTH OF BLANKET
10.16 MM (0.40")
LENGTH OF BLANKET
10.16 MM (0.40")

4(a)

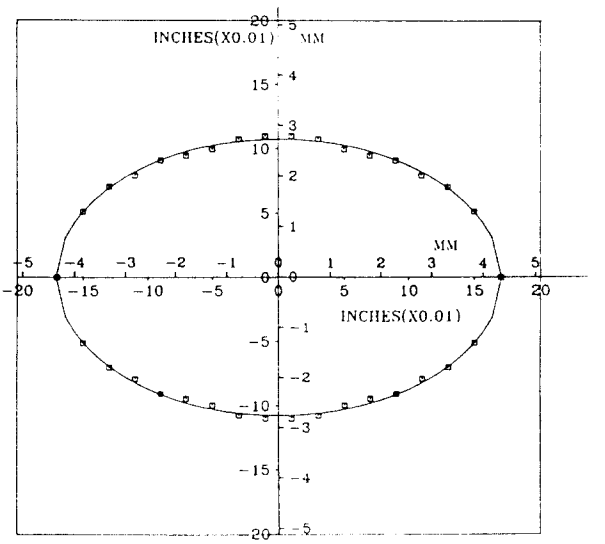
INCHES(X0.01)
MM
MM
INCHES(X0.01)

4(b)

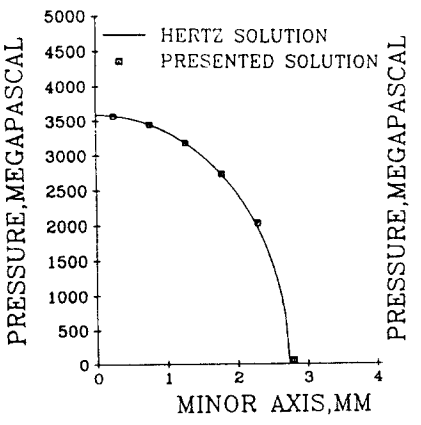
HERTZ SOLUTION
PRESENTED SOLUTION
PRESSURE,MEGAPASCAL
MINOR AXIS,MM

4(c)

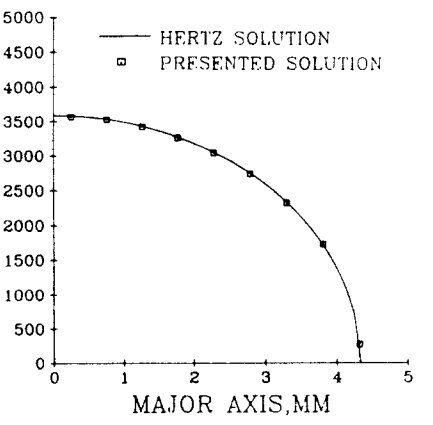
HERTZ SOLUTION
PRESENTED SOLUTION
MAJOR AXIS,MM

4(d)

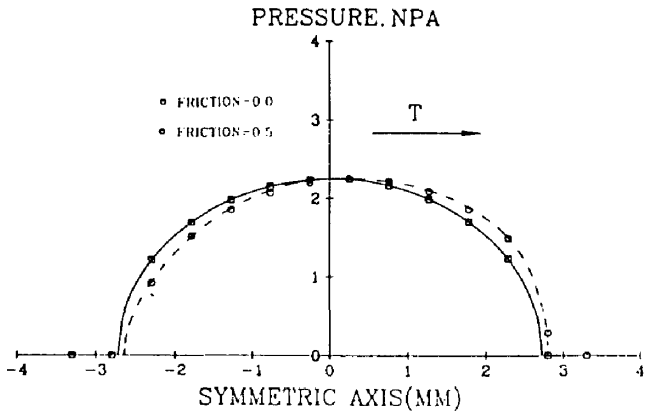

4(e)

Fig. 4. Hertzian contact problem. (R_y = 50.8 mm (2 in.), R_x = 101.6 mm (4 in.), P = 88.96 kN (20,000 lb.) (a) Stress distribution. (b) Contact region (line—Hertz solution; square—present solution). (c) Stress distribution along major axis (line—Hertz solution; square—present solution). (d) Stress distribution along minor axis (line—Hertz solution; square—present solution). (e) Stress distribution along major axis; comparison between friction (μ = 0.5 circles) and nonfriction (squares) cases.

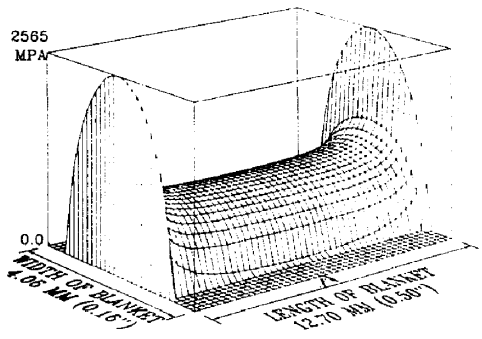

5(a)

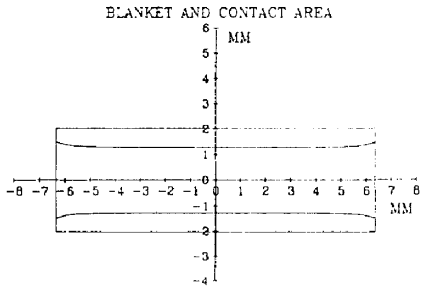

5(b)

Fig. 5. Stress distribution for half space indented by rigid right circular cylinder. (P = 26.70 kN (6000 lb.), $R_y = \infty$, R_x = 50.8 mm (2.0 in.) (a) Stress distribution. (b) Contact region.

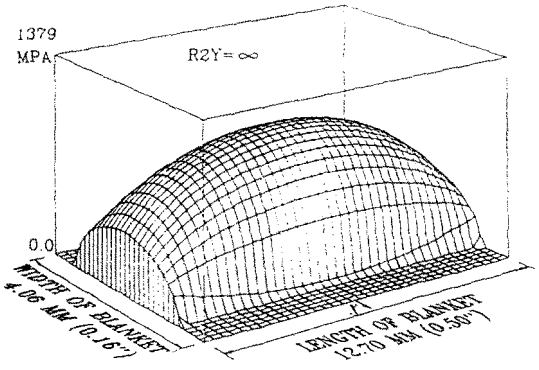

6(a)

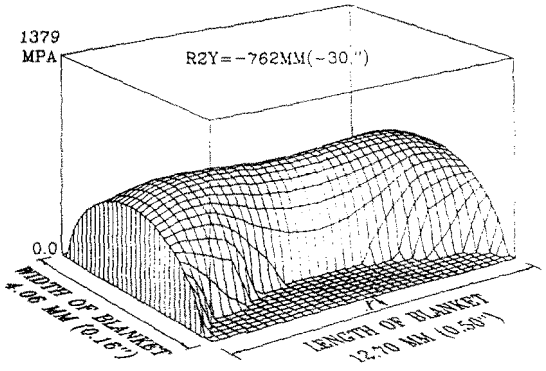

6(b)

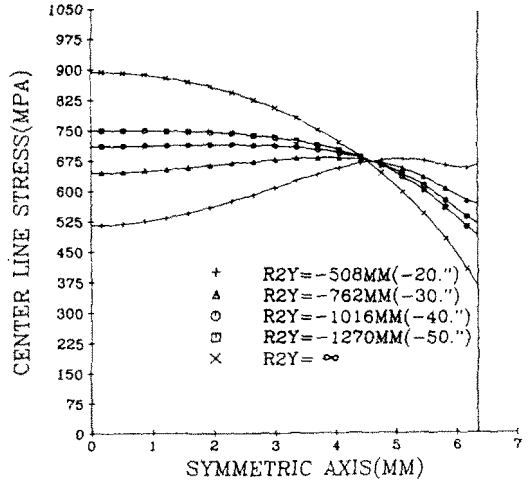

6(c)

Fig. 6. Pressure distribution (p') for half space indented by rigid right circular cylinder. ($P = 26.70$ kN (6000 lb.) (a) $R_x = 50.8$ mm (2.0 in.), $R_y = \infty$. (b) $R_x = 50.8$ mm (2.0 in.), $R_y = -762$ mm (−30 in.). (c) Center line p' distribution for various values of R_y.

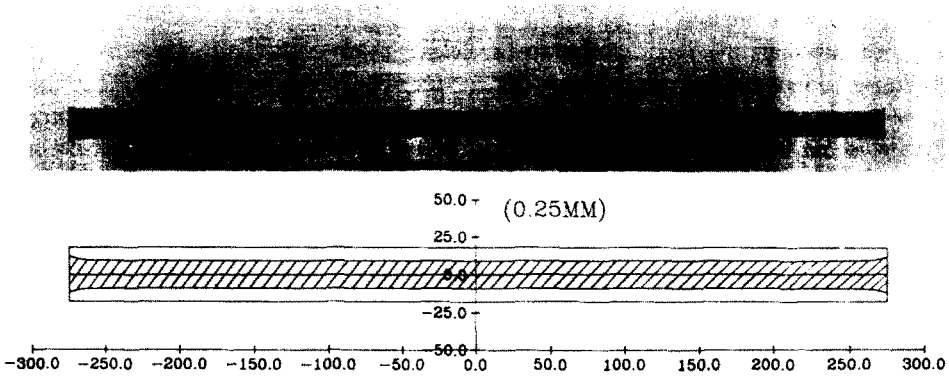

7(a)

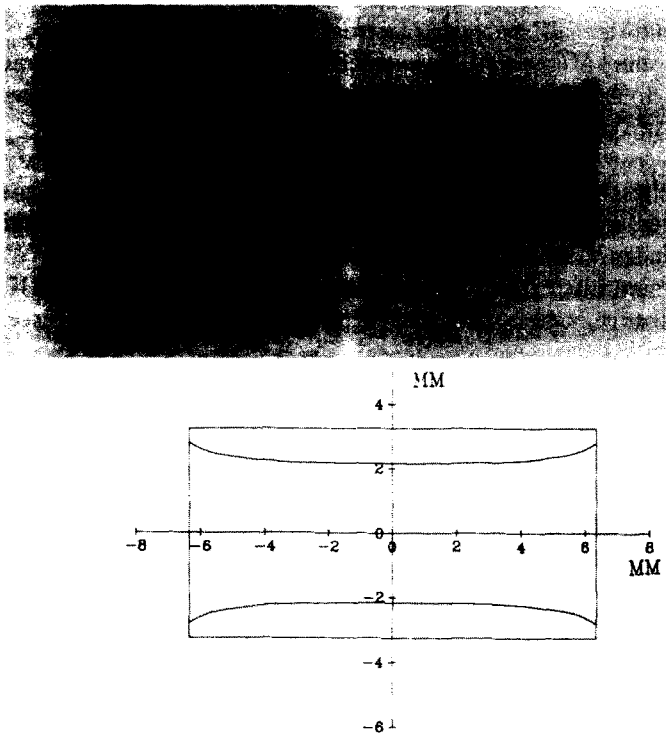

7(b)

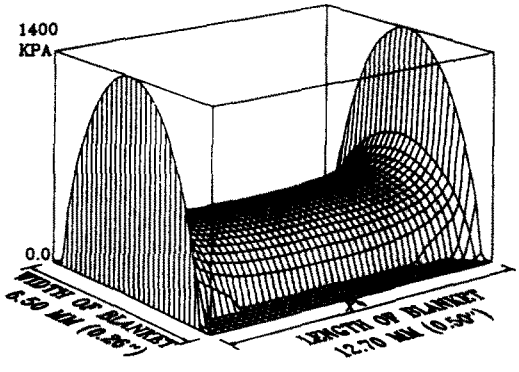

7(c)

Fig. 7. Comparison of contact area between theory and experiment. $R_y = \infty$, $R_x = 12.7$ mm (0.5 in.), $E = 3.45$ MPa (500 psi), $\nu = 0.474$ (a) $l = 12.7$ mm (0.5 in.), (b) $l = 139.7$ mm (5.5 in.), (c) Pressure distribution (Case (a)).

Aligned cylinder with friction†

Here, we consider the rigid cylinder to be sliding in an elastic half space in a direction perpendicular to its axis (x-direction) and with $\mu = 0.8$. The results are plotted in Figs. 8(a, b) in which the form of pressure at the edges remains the same, but the shape of the pressure distribution is no longer symmetric and the maximum pressure has moved from the center slightly opposite to the direction of the frictional force (also see Fig. 4e) of the cylinder on the half space.

Next, we consider the friction to be in the direction of the cylinder axis. For this case the effect of sliding will cause changes in the stress distribution and contact area. The pressure at the edge in the direction of the sliding will decrease, while that in the direction opposite to the sliding will increase; the amount of the change will depend upon the value of μ. The contact area and the pressure distribution for this case are shown in Figs. 9(a, b).

Misaligned cylinder (frictionless)†

In this case the cylinder is not parallel to the half space, and its axis makes an angle θ with the plane of the half space. By changing the value of θ, the shape of the pressure at the edge which is indented less into the half space will decrease and for a certain value of θ_0, it will become zero. For larger values of θ we will have a receding contact situation. Examples of this are shown in Figs. 10(a, b) and Figs. 11(a, b). We note in Fig. 10 that even a relatively small slope can produce a drastic change in the contact area.

Conical cylinder (frictionless)†

In this case a truncated cone is pressed into the half space such that only its side makes contact. The conical cylinder is defined by two end surfaces of radii, $R_{1x} = 5.08$ mm (0.2 in.) and $R_{2x} = 12.70$ mm (0.5 in.), and it is pressed into the half space with a force of 7.22 N (1.50 lb.). From Fig. 12 it is clear that the highest stress will occur at the end with the smallest radius.

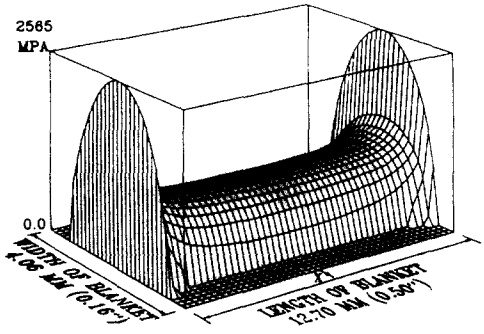

8(a)

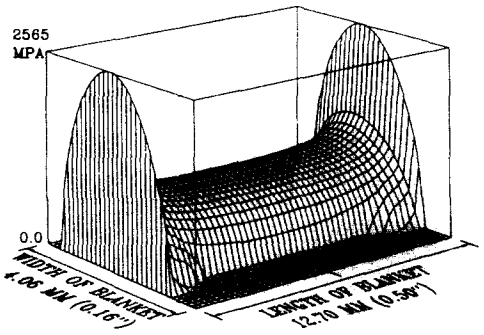

8(b)

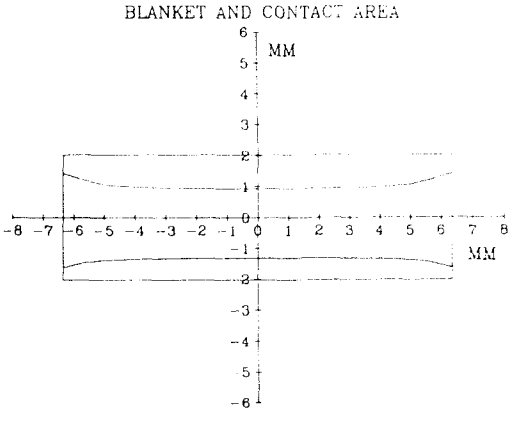

8(c)

Fig. 8. Stress distribution for a half space indented by cylinder with friction in the direction perpendicular to the axis. $P = 26.70$ kN (6000 lb.), $R_y = \infty$, $R_x = 50.8$ mm (2.0 in.), $l = 12.7$ mm (0.50 in.). Figs. (a) and (b) show different views.

†Here, the stresses at the cylinder's sharp edges are not calculated with eqns (25)–(27). Except for stress intensification factor the stress calculation should produce accurate results.

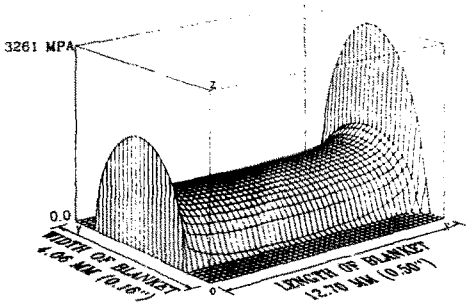

9(a)

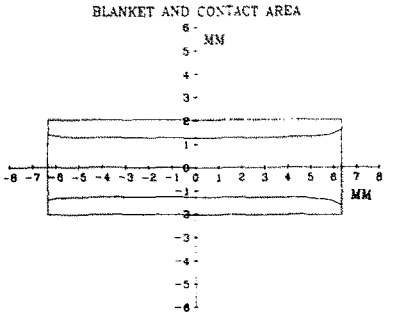

9(b)

Fig. 9. Contact problem for cylinder with friction in direction of axis. $R_y = \infty$, $R_x = 50.8$ mm (2.0 in.), $\mu = 0.8$, $P = 26.70$ kN (6000 lb.), $l = 12.70$ mm (0.50 in.). (a) Pressure distribution (friction on half space is in $-x$ direction, (b) Contact area.

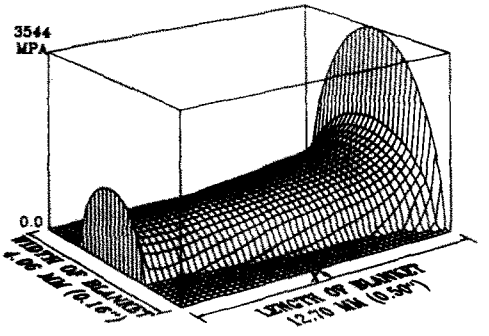

10(a)

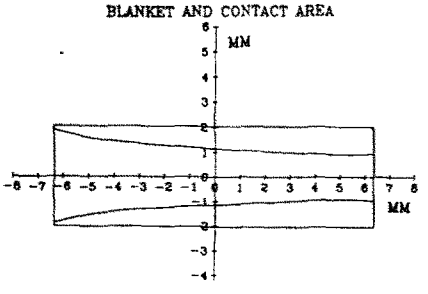

10(b)

Fig. 10. Frictionless contact for cylinder with slope angle = 0.003. $R_y = \infty$, $R_x = 50.8$ mm (2 in.), $P = 26.70$ kN (6000 lb.), $l = 12.70$ mm (0.50 in.). (a) Pressure distribution, (b) Contact area.

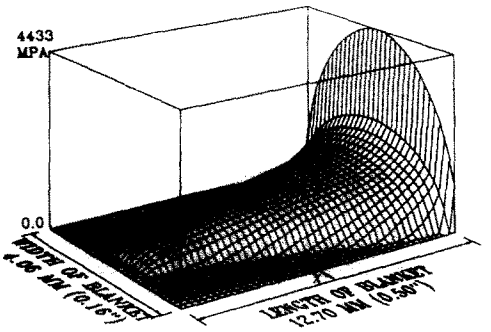

11(a)

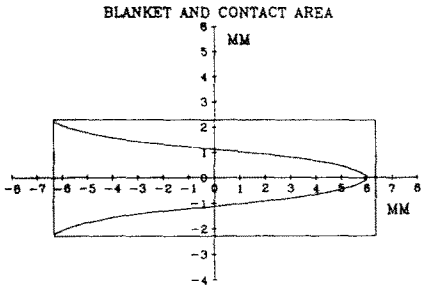

11(b)

Fig. 11. Frictionless contact for cylinder with slope angle = 0.006. $R_y = \infty$, $R_x = 50.80$ mm (2 in.), $P = 26.70$ kN (6000 lb.), $l = 12.70$ mm (0.50 in.). (a) Pressure distribution, (b) Contact area.

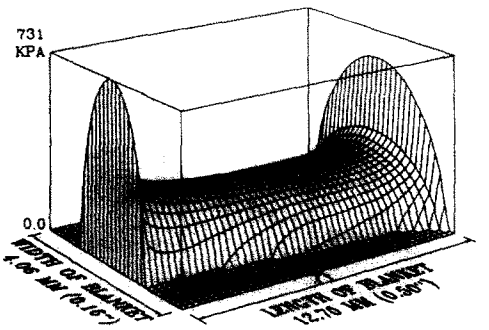

12(a)

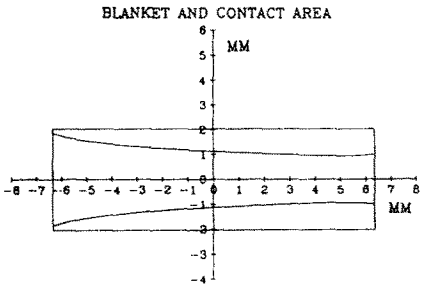

12(b)

Fig. 12. Frictionless contact for conical cylinder. $R_y = \infty$, $R_{1x} = 5.08$ mm (0.2 in.), $R_{2x} = 12.70$ mm (0.5 in.), $P = 7.22$ N (1.50 lb.), $l = 12.7$ mm (0.50 in.), $E = 500$ psi (3.45 MPa), $\nu = 0.474$. (a) Pressure distribution, (b) Contact area.

Acknowledgement—The authors are grateful to the National Science Foundation, grant CME 7918015, for the support of this research.

REFERENCES

1. T. F. Conry and A. Seireg, A mathematical programming method for design of elastic bodies in contact. *J. Appl. Mech.* **38**, 387–392 (1971).
2. M. J. Hartnett, A general numerical solution for elastic body contact problems. *Solid Contact and Lubrication* (Edited by H. S. Cheng and L. M. Keer), Vol. **39**, pp. 51–66, ASME AMD (1980).
3. H. Hertz, *Miscellaneous Papers, on the Contact of Elastic Solids*, Translation by Jones, D. E. McMillan, London (1896).
4. T. G. Johns and A. W. Leissa, The normal contact of arbitrary shaped multilayered elastic bodies. *The Mechanics of the Contact Between Deformable Bodies* (Edited by A. D. de Pater and J. J. Kalker), pp. 254–264. Delft Univ. Press (1975).
5. J. J. Kalker, On elastic line contact. *J. Appl. Mech.* **39**, 1125–1132 (1972).
6. J. J. Kalker, Variational principles of contact elastostatics. *J. Inst. Maths. Applies* **20**, 199–219 (1977).
7. J. J. Kalker, The computation of three-dimensional rolling contact with dry friction. *Int. J. Num. Meth. Engng* **14**, 1293–1307 (1979).
8. J. J. Kalker, H. J. C. Allaert and J. de Mul, The numerical calculation of the contact problem in the theory of elasticity. *Non-linear finite element analysis in structural mechanics* (Edited by Wunderlich, Stein, Bathe). Springer, Berlin (1981).
9. A. E. H. Love, *Elasticity*, 4th Edn. Dover Publication, New York (1944).
10. R. D. Mindlin, Compliance of elastic bodies in contact. *J. Appl. Mech.* **16**, 259–268 (1949).
11. K. P. Oh and E. G. Trachman, A numerical procedure for designing profiled rolling elements. *J. Lub. Techn.* **98**, 547–552 (1976).
12. B. Paul, J. Hashemi, An improved numerical method for counterformal contact stress problems. Rep. U.S. Dept. Transport, FRA/ORD-78/26.
13. H. Reusner, Druckflächenbelastung und Oberflächenverschiebung im Wälzkontakt von Rotations körpern, SKF Schweinfurt (1978) (in German).
14. K. P. Singh and B. Paul, Numerical solution of non-hertzian elastic contact problems. *J. Appl. Mech.* **41**, 484–490 (1974).
15. H. A. Tomas and V. A. Hoersch, Stresses due to the pressure on one elastic solid on another. Bull. Engng Experiment Station, No. 212. University of Illinois, 1930.